J|A|C|S
ARTICLES
Published on Web 09/18/2002

Optical and Photophysical Properties of Light-Harvesting Phenylacetylene Monodendrons Based on Unsymmetrical Branching

Joseph S. Melinger,*,† Yongchun Pan,‡ Valeria D. Kleiman,†,§ Zhonghua Peng,*,‡ Benjamin L. Davis,†,|| Dale McMorrow,† and Meng Lu‡

Contribution from the Electronics Science and Technology Division, Naval Research Laboratory, Code 6812, Washington, D.C. 20375, and Department of Chemistry, University of Missouri-Kansas City, 5100 Rockhill Road, Kansas City, Missouri 64110

Received March 14, 2002

Abstract: The optical and photophysical properties of phenylacetylene dendritic macromolecules based on unsymmetrical branching are investigated using steady-state and time-dependent spectroscopy. Monodendrons, up to the fourth generation, are characterized with and without a fluorescent perylene trap at the core. The higher generation monodendrons without the perylene trap exhibit high molar extinction coefficients ($>10^5$ M^{-1} cm^{-1}) and high fluorescence quantum yields (65−81%). When a perylene trap is placed at the core, then the monodendrons typically exhibit high energy transfer quantum yields (∼90%), as well as subpicosecond time scale excited-state dynamics, as evidenced by ultrafast pump−probe measurements. The photophysical properties of the unsymmetrical monodendrons are compared to those of phenylacetylene monodendrons with symmetrical branching, which have been described recently. The high fluorescence quantum yields and large energy transfer quantum efficiencies exhibited by the unsymmetrical monodendrons suggest they have potential for applications in molecular-based photonics devices.

Introduction

Dendrimer macromolecules recently have attracted considerable attention as novel materials for synthetic light-harvesting systems.[1−8] There are two characteristics of the dendrimer architecture that are central to its light-harvesting ability. First, the dendrimer possesses a highly branched structure that radiates out from a central core. The dendritic structure mimics that of trees found in nature and, thus, appears well suited to efficiently funnel energy to a single site. Second, the high density of sites at the periphery can be functionalized with chromophore groups, forming the basis for an efficient light-absorbing molecular antenna. The light-harvesting action in a dendrimer occurs by rapid transport of energy absorbed at the periphery, through the dendritic branches to the core, where it may then be used to trigger a subsequent event.

To date, efficient light-harvesting dendrimers have been demonstrated using two different approaches. In one approach developed by Fréchet and co-workers,[3] a flexible poly(aryl)-ether dendrimer is functionalized with dye molecules at the periphery, which serve as the molecular antenna, while the core is functionalized with a suitable dye molecule that serves as the energy acceptor. The poly(aryl)ether framework forms a transparent spacer to separate the donor groups at the periphery from the acceptor at the core. Energy transfer occurs primarily by a through-space Förster-type mechanism, and energy transfer quantum yields greater than 90% have been measured for dendrimer sizes up to the fourth generation.[8] In the other approach, the entire dendrimer framework serves both as the light-absorbing antenna and as an energy transport medium. In particular, Moore and co-workers have developed a series of monodendrons (the monodendron represents a single wedge of the full dendrimer macromolecule, which typically contains 2−4 monodendrons of identical chemical structure attached at the core) based on linear phenylacetylene (PA) chains that are specially arranged to form an energy gradient.[2,9] Here, the

* To whom correspondence should be addressed. E-mail: (J.S.M) melinger@ccf.nrl.navy.mil; (Z.P.) pengz@umkc.edu.
† Naval Research Laboratory.
‡ University of Missouri − Kansas City.
§ Current address: Department of Chemistry, University of Florida, Gainesville, FL 32611-7200.
|| National Research Council Postdoctoral Associate.

(1) Denti, G.; Campagna, S.; Serroni, S.; Ciano, M.; Balzani, V. *J. Am. Chem. Soc.* **1992**, *114*, 2944.
(2) Devadoss, C.; Bharathi, P.; Moore, J. S. *J. Am. Chem. Soc.* **1996**, *118*, 9635.
(3) Gilat, S. L.; Adronov, A.; Fréchet, J. M. J. *Angew. Chem., Int. Ed.* **1999**, *38*, 1422.
(4) Schenning, A. R. H. J.; Peeters, E.; Meijer, E. W. *J. Am. Chem. Soc.* **2000**, *122*, 4061.
(5) (a) Peng, Z.; Pan, Y.; Yu, B.; Zhang, J. *J. Am. Chem. Soc.* **2000**, *122*, 6619. (b) Pan, Y.; Lu, M.; Peng, Z. *Polym. Mater. Sci. Eng.* **2001**, *84*, 780.
(6) Sato, T.; Jiang, D.-L.; Aida, T. *J. Am. Chem. Soc.* **1999**, *121*, 10658.
(7) For a review of light-harvesting dendrimers, see: Adronov, A.; Fréchet, J. M. J. *Chem. Commun.* **2000**, 1701.
(8) Adronov, A.; Gilat, S. L.; Fréchet, J. M. J.; Ohta, K.; Neuwahl, F. V. R.; Fleming, G. R. *J. Am. Chem. Soc.* **2000**, *122*, 1175.
(9) (a) Kopelman, R.; Shortreed, M. R.; Shi, Z. Y.; Tan, W.; Xu, Z.; Moore, J. S. *Phys. Rev. Lett.* **1997**, *78*, 1239. (b) Shortreed, M. R.; Swallen, S. F.; Shi, Z.-Y.; Tan, W.; Xu, Z.; Devadoss, C.; Moore, J. S.; Kopelman, R. *J. Phys. Chem. B* **1997**, *101*, 6318.

10.1021/ja020380j CCC: $22.00

Chart 1. Unsymmetrical OH-Terminated Phenylacetylene Monodendrons, GnOH

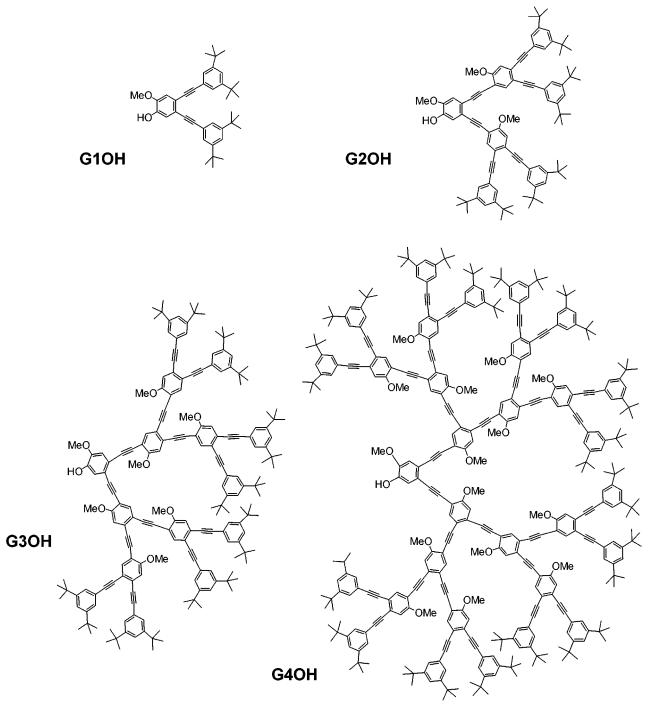

conjugation length of the PA chains increases in the direction toward the core, which leads to rapid and directional energy transport, and results in an energy transfer quantum yield that approaches unity.[2] The nature of the energy gradient in PA monodendrons has been examined theoretically[10,11] and experimentally with a variety of techniques including steady-state absorption and fluorescence spectroscopy,[2,9] picosecond time-resolved fluorescence,[12] and, more recently, ultrafast pump−probe spectroscopy.[13]

To date, most dendrimers that have been studied have a symmetrical branching structure; that is, the branches that radiate out toward the periphery are structurally equivalent. In this paper, we investigate the photophysical properties of a new type of PA monodendron that is characterized by unsymmetrical branching points (see Charts 1 and 2); that is, the branches that extend outward are structurally nonequivalent. The synthesis and a preliminary account of the optical properties of the unsymmetrical monodendrons have been presented recently.[5] The distinction between symmetrical and unsymmetrical monodendrons is illustrated using the model structures shown in Figure 1.

The different types of branching produce significantly different optical and photophysical properties. For example, the compact PA monodendrons (as defined in ref 9, the compact form is structurally symmetric with each branch consisting of a diphenylacetylene unit; the extended form differs in that it has branches consisting of PA chains of increasing length toward the center) synthesized and studied by Moore, Kopelman, and

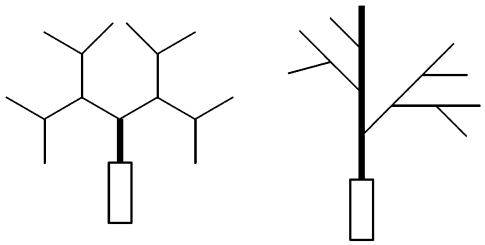

Figure 1. Model structures of monodendrons with (A) symmetrical branching and (B) unsymmetrical branching.

co-workers[2,9] are characterized by symmetrical branching, which results from substitution entirely at the *meta* positions of the benzene ring (see Chart 2). The all-*meta* branching disrupts the π-electron conjugation between any pair of branches,[9a,11a] so, to a first approximation, the electronic excitations are localized on individual branches that consist of diphenylacetylene-like chromophores. Because of the localization, the absorption spectrum of the compact PA monodendron (as well as the full dendrimer) resembles that of diphenylacetylene. In contrast, the unsymmetrical monodendrons studied here are characterized by branching at the *ortho* and *para* positions of the benzene ring when using the direction from dendritic periphery to the core as a reference (see Chart 1). Equivalently, the branching could be described as occurring at the *meta* and *para* positions in the direction from the core to the periphery. One effect of unsymmetrical branching is that it leads to rapidly increasing conjugation lengths of the PA chains as the generation number is increased. Thus, broad absorption spectra are anticipated for unsymmetrical PA monodendrons. Further, because "short-cuts" exist between the peripheral chains and the core (that is, the smallest PA chains are in some cases directly attached to the longest chain that leads to the dendritic core), it may also be anticipated that the time scale and mechanism of energy transport will be different from dendritic macromolecules with symmetrical branching.

In this paper, we present a detailed photophysical characterization of unsymmetrical PA monodendrons in solution. The techniques of steady-state absorption and fluorescence spectroscopy, time-dependent fluorescence spectroscopy, and ultrafast degenerate pump−probe spectroscopy are used to characterize the monodendrons. The absorption and fluorescence properties are also characterized in different solvent environments. Where appropriate, we compare the photophysical properties of the unsymmetrical PA monodendrons to those of the symmetrical PA monodendrons studied previously.

Experimental Section

A brief account of the synthetic approaches to the unsymmetrical monodendrons has been published previously,[5] and a more detailed description of the synthetic procedures will be reported separately. All compounds and purities were confirmed by spectroscopic methods. All solvents used in the spectroscopic measurements were either HPLC grade or spectroscopic grade and were used as received. For comparison purposes, the absorption spectra of the compounds diphenylacetylene, and the isomers 1,2-, 1,3-, and 1,4-bis(phenylethynyl)benzene, were characterized. Diphenylacetylene and 1,2-bis(phenylethynyl)benzene were purchased from Aldrich and purified before use. 1,3-, and 1,4-bis(phenylethynyl)benzene were synthesized by Sonogashira coupling of the appropriate diiodobenzene with (trimethylsilyl)acetylene, followed by desilylation with tetrabutylammonium fluoride.

(10) Bair-Haim, A.; Klafter, J.; Kopleman, R. *J. Am. Chem. Soc.* **1997**, *119*, 6197.
(11) (a) Tretiak, S.; Chernyak, V.; Mukamel, S. *J. Phys. Chem. B* **1998**, *102*, 1239. (b) Kirkwood, J.; Schuerer, C.; Mukamel, S. *J. Chem. Phys.* **2000**, *2414*, 2001.
(12) Swallen, S. F.; Kopelman, R.; Moore, J. S.; Devadoss, C. *J. Mol. Struct.* **1999**, *485*, 585.
(13) Kleiman, V.; Melinger, J. S.; McMorrow, D. *J. Phys. Chem. B* **2001**, *105*, 5595.

Chart 2. Unsymmetrical Perylene-Terminated Phenylacetylene Monodendrons, GnPer, and Fourth Generation Symmetrical Perylene-Terminated Monodendrons: A Compact Phenylacetylene Monodendron **1** and an Extended Phenylacetylene Dendritic Macromolecule **2**

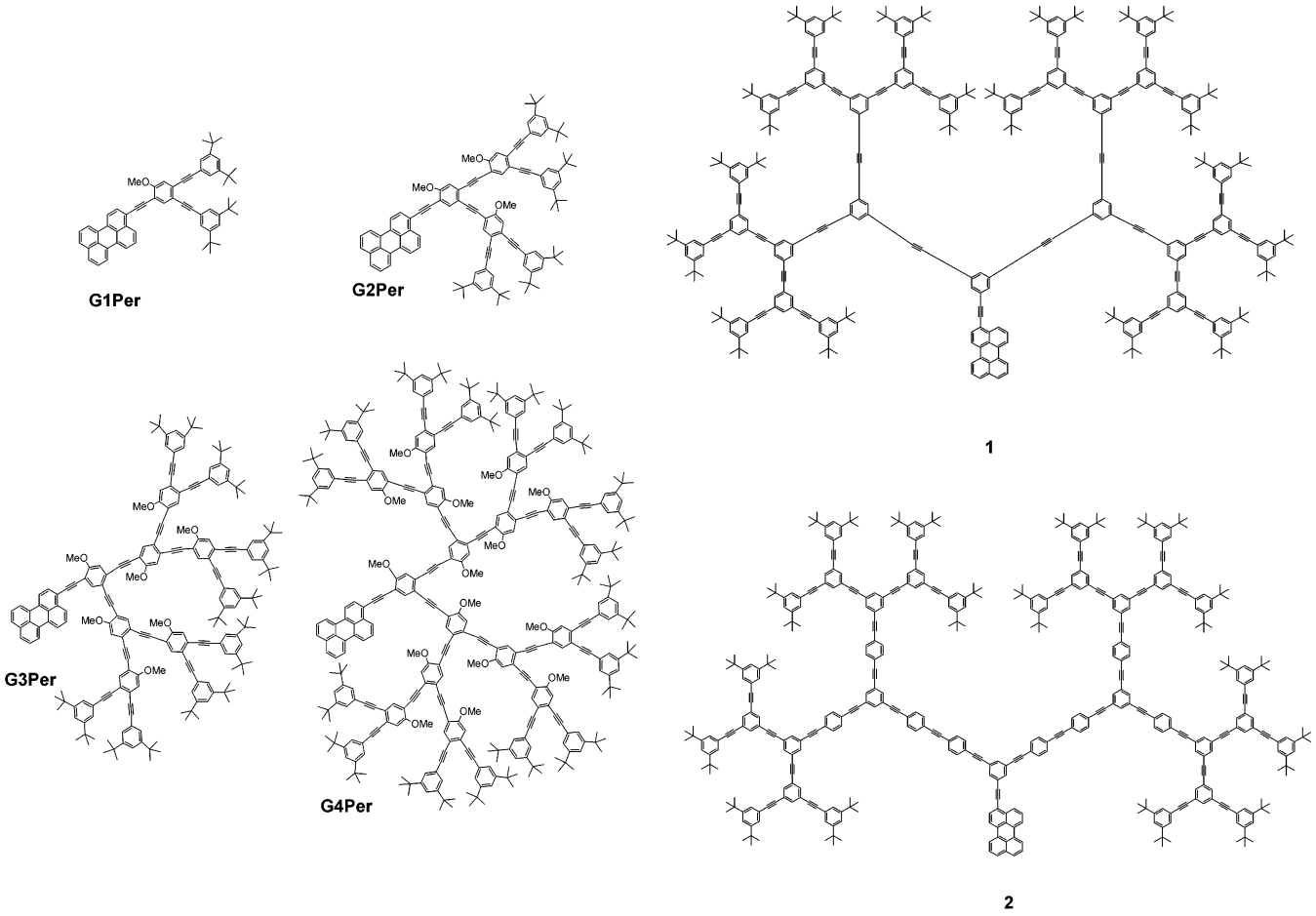

UV−vis absorption spectra were recorded in 1 cm path length UV-grade spectrophotometric cells using a Perkin-Elmer Lambda 5 absorption spectrometer. The fluorescence emission and excitation spectra were measured using a SPEX Fluorolog spectrometer (model 1680) equipped with a double monochromator on the emission side of the instrument. The same UV-grade cells used for the absorption measurements were used in emission experiments. All samples were deoxygenated by bubbling N_2 gas through the sample immediately prior to the fluorescence measurements. The slits on the excitation and emission sides of the fluorescence spectrometer were set to a band-pass of 1.3 nm, and all spectra were corrected for wavelength variations of the excitation lamp, photomultiplier response, and the optical components. The sample concentrations were adjusted to keep the optical density below 0.10 in a 1 cm path length. Fluorescence quantum yields were determined by comparing the integrated fluorescence spectra of the monodendrons with the integrated fluorescence spectrum of quinine sulfate in 1 N H_2SO_4 ($\phi_{fl} \approx 0.55$),[14] and then by correcting for the different refractive indices of the sample and the standard. The refractive index of the solvent was used to approximate the sample refractive index, and the refractive index of water was used for the standard (both at 25 °C).

The time-dependent fluorescence measurements were performed using the technique of time-correlated single photon counting (TCSPC). The laser excitation source consisted of a synchronously pumped and cavity-dumped dye laser (Rhodamine 590) that was pumped by the second harmonic (527 nm) of a Nd:YLF laser operating at 100 MHz. The dye laser contained a single plate birefringent filter that was tuned to produce laser oscillation at 600 nm. The dye laser was cavity-dumped at 1 MHz, and then frequency doubled using a potassium dihydrogen phosphate (KDP) nonlinear crystal. A polarizer was placed between the doubling crystal and the sample to ensure an excitation beam with a well-defined polarization. The fluorescence from the sample was spectrally filtered with a monochromator and detected with a cooled microchannel plate photomultiplier (Hamamatsu # R2809U-11). The fluorescence transients were measured at the magic angle (54.7°).[15] The temporal response function of the system was measured by replacing the sample with a ground glass surface or a cell with a scattering solution. Both gave a response function with a full-width at half-maximum (fwhm) of about 100 ps.

Ultrafast degenerate pump−probe spectroscopy was performed using a kilohertz regeneratively amplified titanium sapphire laser system operating at 800 μJ per pulse at 800 nm, and a temporal width of about 120 fs (fwhm). The output of the titanium sapphire system was used to pump a tunable optical parametric amplifier (OPA). The signal beam of the OPA was upconverted to 310 nm using two stages of frequency doubling with beta barium borate (BBO) crystals. The time duration of the UV pulses was typically less than 180 fs. The UV beam was split into a pump beam and a weaker probe beam (less than 5% of the pump). The probe beam was delayed using a computerized translation stage and then spatially overlapped with the pump beam at the sample. The polarizations of pump and probe beams were oriented parallel. The sample solution was flowed through a 1 mm path length cell, and the optical density was kept below 0.4. The laser pump fluence was kept below 50−60 μJ/cm^2.

(14) Demas, J. N.; Crosby, G. A. *J. Phys. Chem.* **1971**, *75*, 991.

(15) O'Connor, D. V.; Phillips, D. *Time Correlated Single Photon Counting*; Academic Press: New York, 1984.

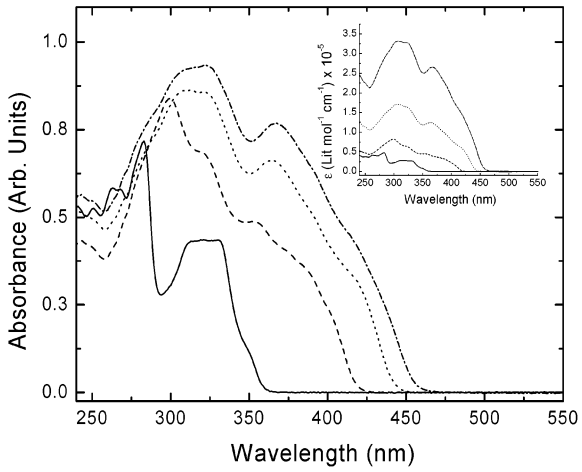

Figure 2. Absorption spectra of GnOH in dichloromethane. G1OH (solid line), G2OH (dashed line), G3OH (dotted line), G4OH (dashed−dotted line). The intensities have been scaled to view the features of each spectrum. Inset: wavelength dependence of the molar extinction coefficients for GnOH in dichloromethane. Concentrations are 6.3×10^{-6} M (G1OH), 3.6×10^{-6} M (G2OH), 1.8×10^{-6} M (G3OH), and 9.0×10^{-7} M (G4OH).

Results and Discussion

Steady-State Absorption. Charts 1 and 2 show the series of unsymmetrical PA monodendrons studied in this paper. Chart 1 shows the OH-terminated structures, GnOH, for $n = 1-4$. These monodendrons represent the model donor compounds. Chart 2 shows the series of perylene-terminated monodendrons, GnPer, for $n = 1-4$. For comparison, Chart 2 also shows the structure of the symmetrical fourth generation compact (**1**) and extended (as defined in ref 9, the compact form is structurally symmetric with each branch consisting of a diphenylacetylene unit; the extended form differs in that it has branches consisting of PA chains of increasing length toward the center) (**2**) perylene-terminated monodendrons.

In the following, all spectroscopic measurements are carried out in dichloromethane (DCM). To complement the measurements in DCM, many of the spectroscopic measurements are also performed in the lower dielectric solvent isopentane (IP). (Absorption spectra, fluorescence spectra, and fluorescence lifetimes of GnOH and GnPer were also measured in pentane and hexane and were found to be nearly identical to those measured in isopentane.) Figures 2 and 3 show the absorption spectra for GnOH in DCM and IP, respectively. The absorption band edge, λ_{edge} (defined here as the wavelength on the band edge that is 5% of ϵ_{max}), the absorption maximum, λ_{max}, and the molar extinction coefficient at λ_{max}, ϵ_{max}, are collected in Table 1. We consider first the absorption spectrum of G1OH in DCM, which may be thought of as the basic building block for the larger generations. The G1OH absorption spectrum shows a λ_{max} at 280 nm and a broad feature centered near 320 nm that extends to the absorption edge near 352 nm. To help in understanding the G1OH spectrum, it is useful to consider the absorption properties of the series of three-ring PA isomers shown in Figure 4 that are distinguished by the type of substitution at the central benzene ring: *meta* (**3**), *para* (**4**), or *ortho* (**5**). As mentioned above, the *meta* branching disrupts the π-electron conjugation; thus, the absorption spectrum of **3** is predicted to resemble the absorption spectrum of diphenylacetylene (DPA). A comparison of the absorption spectra of DPA and **3** shows that, indeed, this is the case: the absorption edge

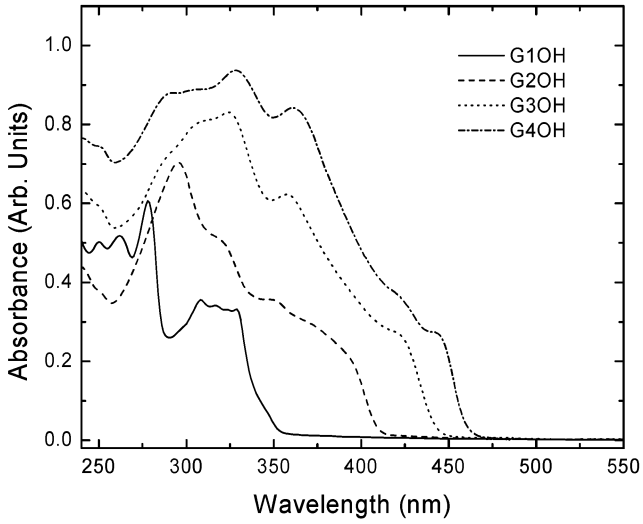

Figure 3. Absorption spectra of GnOH in isopentane. The intensities have been scaled to view the features of each spectrum.

Table 1. Absorption Band Edges (λ_{edge}), Wavelength of the Absorption Maxima (λ_{max}), and Molar Extinction Coefficients at the Absorption Maximum (ϵ_{max}) for GnOH[a]

compd	solvent	λ_{edge} (nm)	λ_{max} (nm)	ϵ_{max} (M^{-1} cm^{-1})
G1OH	DCM	352	283	48 000
	IP	351	278	
G2OH	DCM	416	299	82 500
	IP	409	295	
G3OH	DCM	440	310	171 000
	IP	441	324	
G4OH	DCM	453	321	330 000
	IP	460	328	

[a] Entries left blank indicate that the quantities were not determined for those cases (molar absorptivities in IP were not determined).

of **3** is red-shifted by only 3−4 nm from DPA, and its spectrum largely reproduces the spectral width and vibronic structure displayed by DPA. In contrast, when substitution occurs at the *para* position (**4**), the absorption band edge is red-shifted by 50 nm with respect to the band edge of DPA and appears at 350 nm. The relatively large red shift and loss of the sharp vibronic structure reflect the π-electron delocalization over the linear three-ring chain. The case of *ortho*-substitution is the one most relevant to the G1OH spectrum. The bent three-ring molecule (**5**) exhibits an absorption band edge near 343 nm, which confirms that π-electron delocalization occurs over the bent three-ring chain, although the red shift is somewhat smaller for substitution at the *para* position. The absorption spectra of G1OH and **5** are similar in shape. The red shift of approximately 9 nm for the G1OH spectrum relative to **5** is likely due to the electron-donating effects of the methoxy and hydroxyl groups.

As the generation number is increased, the GnOH absorption spectra shift to the red, and ϵ_{max} increases. The inset to Figure 2 shows that ϵ_{max} approximately doubles with each generation. Thus, the light-collecting efficiency of the PA backbone increases significantly with increasing generation. The absorption edges (in DCM) appear at 352 nm ($n = 1$), 416 nm ($n = 2$), 440 nm ($n = 3$), and 453 nm ($n = 4$). As discussed above, the absorption band edge for G1OH is due to π-electron conjugation over the three-ring bent PA chain. By analogy, we suggest that the absorption edges for the larger monodendrons

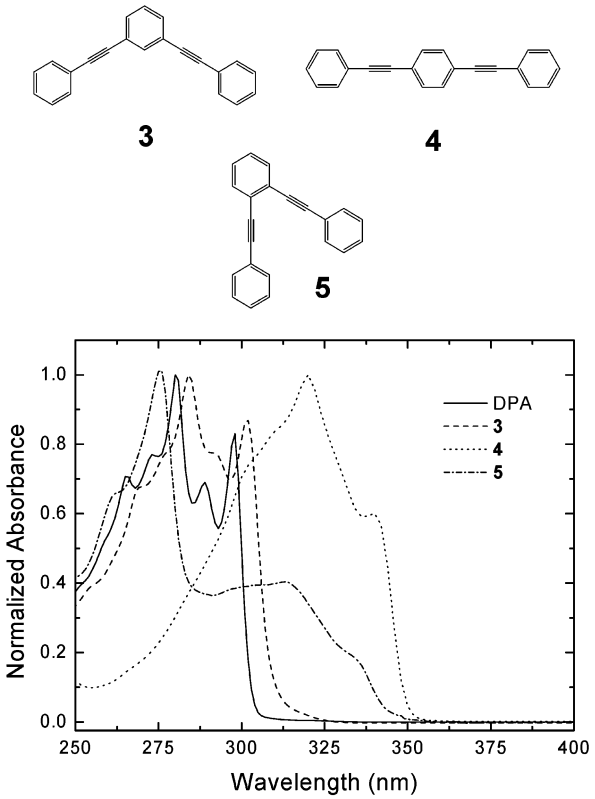

Figure 4. Top: Structures for (**3**) *meta*-, (**4**) *para*-, and (**5**) *ortho*-substituted three-ring phenylacetylenes in dichloromethane. Bottom: Normalized absorption spectra for diphenylacetylene, **3**, **4**, and **5**.

($n \geq 2$) indicate the onset of the absorption due to the longest PA chains over which conjugation is maintained. These correspond to the bent five-ring, seven-ring, and nine-ring PA structures, for G2OH, G3OH, and G4OH, respectively (see Chart 1). Each of these structures includes the central benzene ring at the core that is substituted with an OH group. We emphasize that these assignments are tentative and remain to be tested by theoretical models.

Previous experimental[2,9] and theoretical[11] studies have shown that the symmetrical PA dendrimers exhibit localized electronic excitations. The absorption spectrum of **2**, for example, clearly shows spectral peaks at energies that are characteristic of excitations localized on the two-ring, three-ring, and four-ring PA chains.[9,11a] It is natural to explore the extent to which the unsymmetrical GnOH monodendrons exhibit localized electronic excitations. The chemical structures shown in Charts 1 and 2 suggest that the π-conjugated electronic structure of the unsymmetrical monodendrons is likely to be more complex than the symmetrical monodendrons because of the presence of both *ortho* and *para* branching. Indeed, the absorption spectra of the GnOH series in DCM lack the clear spectral features suggestive of localized electronic excitations. In contrast, however, the GnOH absorption spectra taken in IP show sharper features. Figure 3 shows that the G3OH and G4OH monodendrons exhibit discernible peaks at the red edge of their spectra. Furthermore, in the case of G4OH, the absorption spectrum reveals additional spectral features at wavelengths consistent with the lowest energy spectral peaks observed in G1OH and G3OH. While these observations may be taken as preliminary evidence consistent with the presence of excitations localized on PA chains, a more rigorous comparison of experimental work under higher resolution conditions together with calculations of electronic structure is needed to provide a more definitive conclusion.

Table 2. Absorption Maxima (λ_{max}) and Ratio of Absorption Intensities in the Phenylacetylene Backbone and Perylene Regions for GnPer in Dichloromethane

compd	$\lambda_{max,PA}$ (nm)[a] $\lambda_{max,Per}$ (nm)[b]	$I_{max,PA}/I_{max,Per}$
G1Per	275 482	0.79
G2Per	298 485	1.38
G3Per	304 485	2.35
G4Per	305 486	4.55

[a] $\lambda_{max,PA}$ is the wavelength at the absorption maximum in the phenylacetylene backbone region. [b] $\lambda_{max,Per}$ is the wavelength at the absorption maximum in the perylene region.

The absorption spectra for the GnPer series in DCM are shown in Figure 5a and b, and Table 2 gives the absorption maxima of the PA backbone region ($\lambda_{max,PA}$) and the perylene region ($\lambda_{max,Per}$), and the corresponding ratio of absorption intensities, $I_{\lambda max,PA}/I_{\lambda max,Per}$. The absorption features of the perylene trap can be clearly distinguished from the PA backbone. Figure 5a shows that the absorption band of the perylene trap is red-shifted by approximately 50 nm from that of free perylene in DCM, which indicates that the perylene transition dipole is, to some extent, delocalized into the PA backbone. The sharp peak at 260 nm is due to the $S_2 \leftarrow S_0$ transition (short-axis) of the perylene trap. The absorption from about 275 to 375 nm is primarily due to the G1 pendant because perylene has only a weak absorption in this region (dotted line in Figure 5a). The UV absorption intensity due to the GnPer backbone approximately doubles with each increase in generation number, and the spectra show many of the features seen in the corresponding GnOH spectra. The ratio of $I_{\lambda max,PA}/I_{\lambda max,Per}$ reaches approximately 4.6 for G4Per. A comparison of the absorption spectrum of G4Per to that of the fourth generation symmetrical monodendrons **1** and **2** shows that the ratio $I_{\lambda max,PA}/I_{\lambda max,Per}$ is significantly larger for the symmetrical monodendrons: $I_{\lambda max,PA}/I_{\lambda max,Per} \approx 15.4$ for **1**,[2] and $I_{\lambda max,PA}/I_{\lambda max,Per} \approx 17.8$ for **2**.[9b] The smaller value of $I_{\lambda max,PA}/I_{\lambda max,Per}$ for G4Per is due, in part, to the spreading of the PA backbone absorption over a broader spectral width.

Steady-State Emission. The steady-state fluorescence spectra of GnOH in DCM are shown in Figure 6, and the emission maxima, fluorescence quantum yields, and lifetimes are given in Table 3. The emission spectra were obtained using lamp excitation at 325 nm for G1OH, and at 350 nm for $n \geq 2$. The sample concentration was kept between 2×10^{-6} and 10^{-7} M for all fluorescence measurements. Figure 6 shows that the fluorescence spectra red shift with increasing generation number. Each spectrum shows a relatively sharp peak on the blue side, and a broader peak on the red side, which, for G4OH, extends to about 600 nm. We note that the shape of the GnOH fluorescence spectra is insensitive to changes of excitation wavelength within their absorption profiles.

Fluorescence quantum yields are tabulated in Table 3. The experimental error in determining the fluorescence quantum yields is approximately $\pm 5\%$. In general, the fluorescence

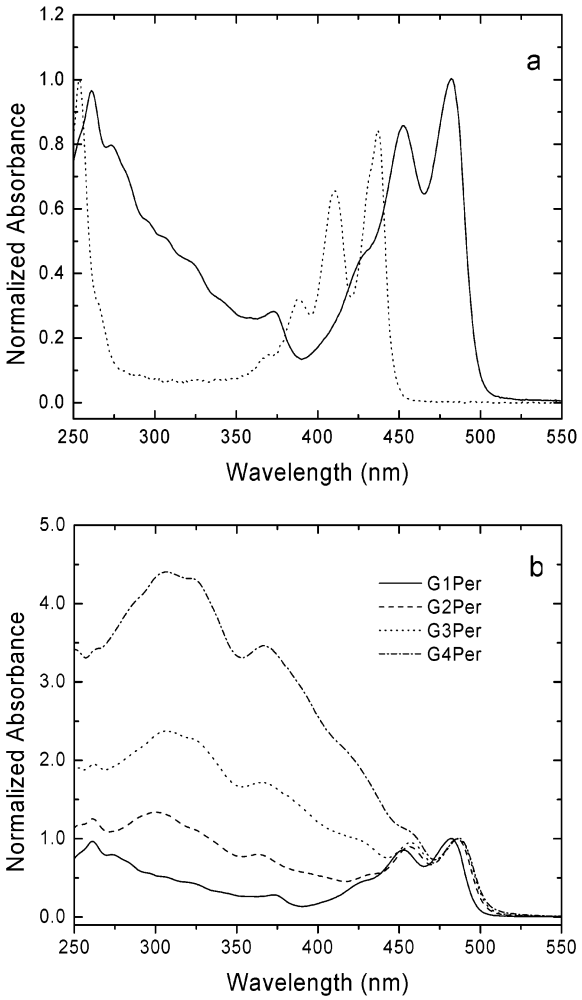

Figure 5. (a) Normalized absorption spectrum for perylene (dotted line) and G1Per (solid line), both in dichloromethane. (b) Absorption spectra of the GnPer series in dichloromethane. Note that the spectra are normalized to unity at the lowest energy peak of the perylene absorption.

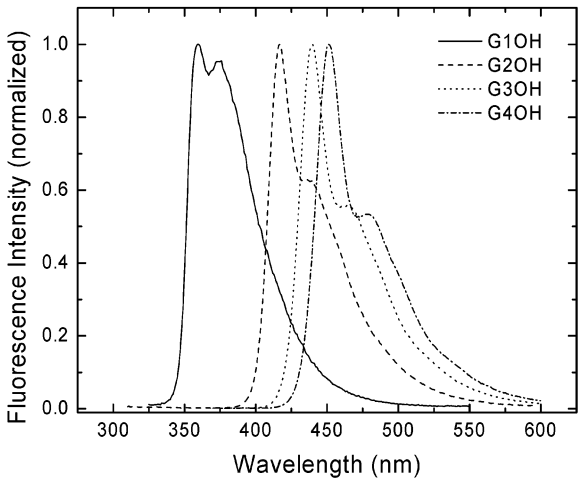

Figure 6. Normalized fluorescence spectra of GnOH in dichloromethane. The excitation wavelength is 325 nm for G1OH and 350 nm for the larger monodendrons.

quantum yields were relatively large, with G2OH exhibiting the highest quantum yield of 81% (in DCM). Even the largest monodendron, G4OH, exhibited a substantial quantum yield of 65% (in DCM). Apparently, interactions between the different

Table 3. Values for λ_{max}, ϕ_{fl}, and the Fluorescence Lifetime for GnOH and GnPer in Dichloromethane and Isopentane[a]

compd	solvent	λ_{max} (nm)	ϕ_{fl}	lifetime (ns)
G1OH[b]	DCM	360, 374 (sh)	0.40	1.7
	IP	351, 368	0.32	1.6
G2OH	DCM	417, 438 (sh)	0.81	2.0
	IP	406, 429 (sh)	0.73	1.9
G3OH	DCM	440, 466 (sh)	0.70	1.9 (97.6%), 3.4 (2.4%)
	IP	435, 464 (sh)	0.70	1.8 (94.4%), 3.0 (5.6%)
G4OH	DCM	452, 479 (sh)	0.65	1.7 (90.7%), 2.7 (9.3%)
	IP	453, 485 (sh)	0.68	1.9 (86.0%), 2.9 (14.0%)
G1Per	DCM	491	0.74	2.2
	IP			
G2Per	DCM	497	0.78	2.0
	IP	484		
G3Per	DCM	498	0.77	1.9
	IP	486		
G4Per	DCM	498	0.74	1.8
	IP	487		1.5 (93.0%), 2.7 (7.0%)

[a] Unless indicated otherwise, the quantum yield measurements were determined using lamp excitation at 350 nm. In the case of biexponential relaxation, the relative amplitudes are given in percent. The lifetime measurements were determined using laser excitation at 300 nm. Entries left blank indicate that measurements were not made for those cases. (sh) indicates shoulder. [b] Quantum yield measurements for G1OH were determined using excitation at 325 nm.

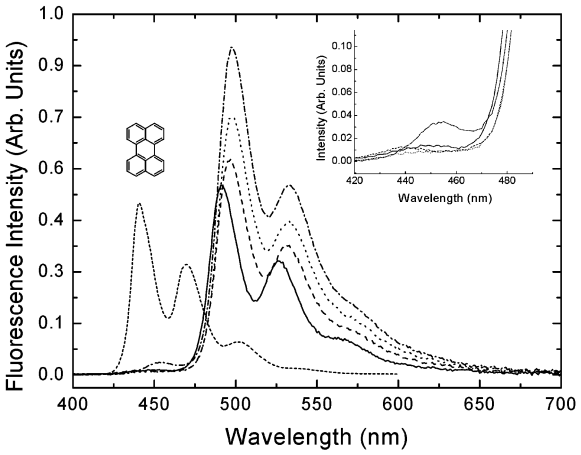

Figure 7. Normalized fluorescence spectra of GnPer in dichloromethane. G1Per (solid line), G2Per (dashed line), G3Per (dotted line), G4Per (dashed−dotted line). The spectrum of free perylene in dichloromethane is also shown (short dashed line). The inset shows the residual emission from the phenylacetylene backbone. The excitation wavelength is 325 nm for G1Per and 350 nm for the larger monodendrons.

branches in the GnOH are not sufficient to significantly quench the fluorescence.

The fluorescence spectra of the GnPer series in DCM are shown in Figure 7, and the fluorescence properties are summarized in Table 3. The excitation wavelength for each monodendron was 350 nm. In each case, the emission originates almost entirely from the perylene trap, which is an important indication that the energy transfer from the PA backbone to the perylene trap is very high. We note that the fluorescence from the perylene trap is red-shifted by about 57 nm from free perylene in DCM, which is consistent with the red shift of the perylene trap observed in the absorption spectrum.

The inset shows the residual emission from the PA backbone on an expanded scale. For generations 1−3, it is evident that less than 2% of the total GnPer emission comes from the PA

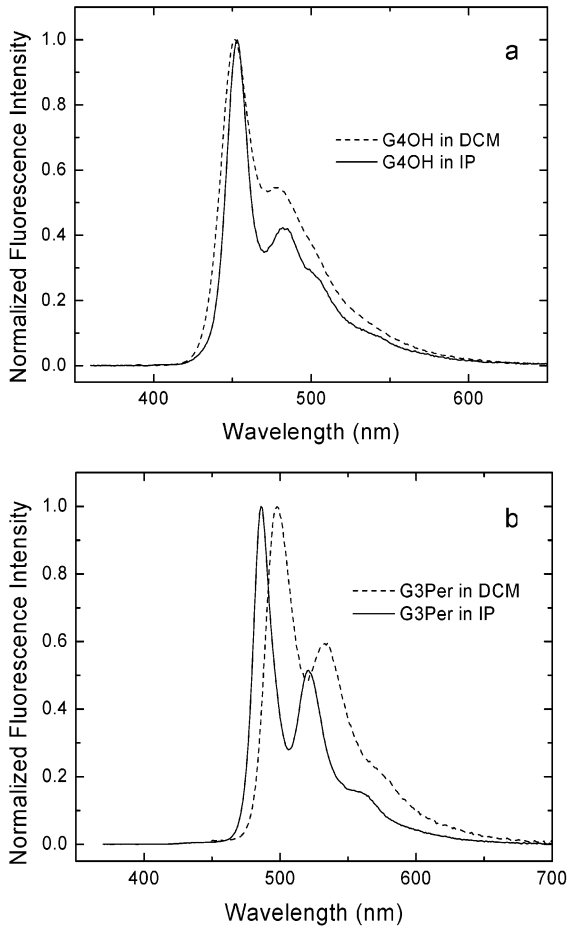

Figure 8. (a) Normalized fluorescence spectra of G4OH in dichloromethane (dashed line) and in isopentane (solid line). (b) Normalized fluorescence spectra of G3Per in dichloromethane (dashed line) and in isopentane (solid line).

backbone region. In the case of G4Per, the emission from the backbone region is greater, but still less than 5% of the total emission. The fluorescence quantum yields for the GnPer series in DCM fall in the 70−80% range, indicating that a large fraction of the energy that is funneled to the perylene trap is converted to fluorescence emission in a relatively small spectral region.

The effect of the solvent environment on the fluorescence properties of the GnOH and GnPer series is studied by measuring the spectra in solvents of increasing dielectric constant: IP (1.9), tetrahydrofuran (THF) (7.5), and DCM (8.9), at 25 °C. For GnOH, the wavelength positions of the fluorescence bands are similar in DCM and THF. In IP, as the generation number is increased, the fluorescence maxima show a gradual shift to the red relative to those taken in DCM. For G4OH, the fluorescence maxima in DCM and IP are nearly the same. The most noticeable difference is that the fluorescence spectra measured in IP are significantly sharper than those in either DCM or THF. As an example, Figure 8a compares the normalized fluorescence spectra for G4OH in IP and DCM. The half-width of the main spectral peak is about 7 nm in IP and 11 nm in DCM. Further, the sharper features of the spectrum in IP show more evidence of a vibrational progression. For GnPer, the emission spectra collected in IP show a blue shift of 12−13 nm relative to the emission spectra taken in DCM and THF, and the fluorescence line shape from the perylene trap in IP is significantly sharper than that in either DCM or THF. These effects are illustrated in Figure 8b, which compares normalized emission spectra for G3Per in IP and DCM. The IP solvent molecules are less polarizable than the DCM molecules and, consequently, interact more weakly with the π-electron system of the monodendron, which explains the sharper features observed in the absorption and emission spectra for IP. Finally, we mention that no evidence of emission from aggregates (for example, excimers) was found from GnOH or GnPer in DCM at monodendron concentrations less than 10^{-6} M. In IP, a concentration-dependent spectral broadening and red shift of the fluorescence occurs for G4Per at concentrations above approximately 10^{-6} M, which is a sign that aggregation is occurring. A spectral broadening and red shifting of the fluorescence was not observed for G4OH in IP at similar concentrations above 10^{-6} M.

It is useful to compare the fluorescence properties of the unsymmetrical GnOH monodendrons to those of the compact symmetrical PA monodendrons (without the perylene trap) studied previously.[2,9] One difference is that the fluorescence spectra of GnOH red shift with increasing generation, whereas the spectra that arise from the series of compact symmetrical monodendrons remain stationary. The red shift is due to the longer conjugated PA chains present in the higher generations, which is a consequence of the unsymmetrical branching. In contrast, the all-*meta* branching in the compact monodendrons localizes the excitations on a single DPA chain and gives rise to a fluorescence spectrum that remains relatively stationary as the generation number increases.[2,9] A second difference is that the fluorescence quantum yields for the GnOH monodendrons are higher (by about a factor of 1.5−3) than those for the compact monodendrons of the same generation (through $n = 4$). Molecular modeling has predicted that the compact PA monodendrons exhibit a globular-like shape.[2,9b] Because of interactions between the various branches, such a structure presumably leads to nonradiative relaxation pathways that compete with the radiative relaxation. While model structures for the GnOH monodendrons remain to be determined, the branching at both *ortho* and *para* positions suggests that the 3D structure becomes increasingly congested as the generation size increases. It's possible that fast energy transfer to the emitting state through an energy gradient helps preserve the high fluorescence quantum yield in GnOH.

Time-Resolved Fluorescence Measurements. The fluorescence dynamics of the GnOH and GnPer series were measured using the technique of time-correlated single photon counting. Each of the samples was excited with an ~1−2 ps laser pulse at 300 nm, and the fluorescence decays were monitored at the emission maximum of each of the samples. The fluorescence lifetimes are given in Table 3 for the monodendrons in DCM and IP. The data were analyzed by fitting the transients to a convolution of the instrument response function and a sum of exponential decay functions. Figure 9 shows an example for the case of G2OH in DCM. The experimental fluorescence decay curve was fit to a single-exponential decay function with a time constant of 2.0 ns, yielding a χ^2 of less than 1.2. The fluorescence decays for the GnPer series in DCM are characterized by a single-exponential fit. Figure 10 shows the fluorescence decay of G3Per overlaid with the decay of free perylene (both in DCM). The fluorescence lifetime of G3Per was found

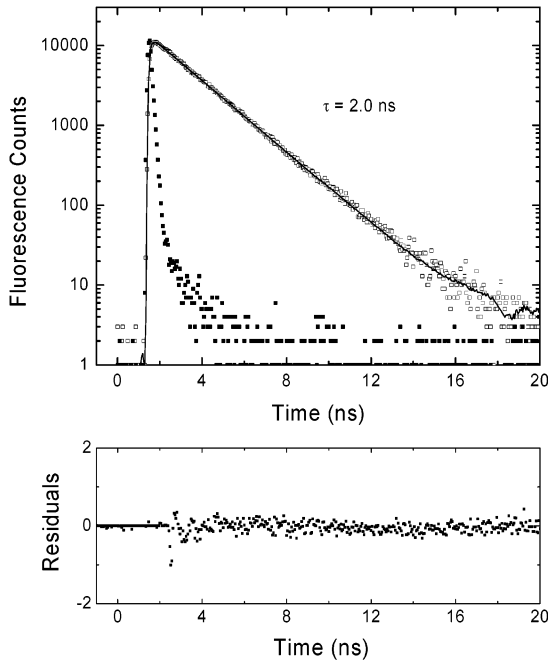

Figure 9. Fluorescence decays in dichloromethane measured by time-correlated single photon counting. (a) The instrument response function (■) and G2OH data (□). The solid line is a fit to the data using a single-exponential decay function ($\tau = 2.0$ ns) that is convoluted with the instrument response ($\chi^2 = 1.19$). The bottom graph shows the residuals.

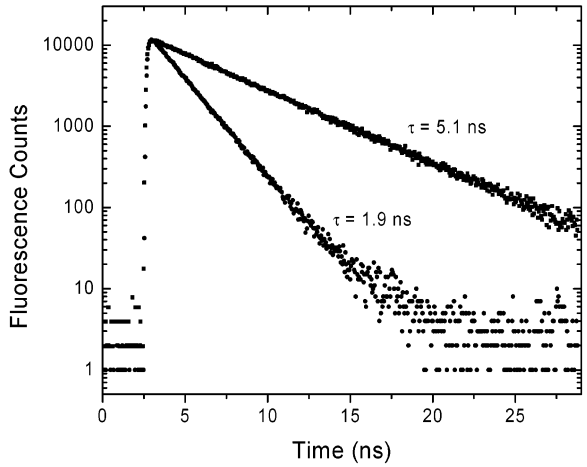

Figure 10. Comparison of the fluorescence decays of G3Per in dichloromethane (●) and free perylene in dichloromethane (■).

to be 1.9 ns, which is to be compared to 5.1 ns for that of free perylene. The shorter lifetime of the perylene emission in G3Per is due to its interaction with the PA backbone.

Inspection of Table 3 shows that the fluorescence decays of G1OH and G2OH in both DCM and IP are characterized by single-exponential time constants. We note that the fluorescence quantum yield doubles in going from G1OH to G2OH but there is not a corresponding increase in fluorescence lifetime. This result may be due to a stronger transition dipole associated with the longer PA chain at the emissive core of the G2OH monodendron. The larger monodendrons, G3OH and G4OH, were better fit by adding a second exponential decay function with a somewhat longer time constant. In DCM, the longer time constant component makes a relatively small contribution (<10%), whereas in IP the relative contribution of the slower component is somewhat larger. The GnOH displays a similar size dependence of the fluorescence decay times in both DCM and IP. There is only a minor decrease (about 15%) of the shorter time constant as the monodendron size is increased beyond $n = 2$. A possible explanation for the observed biexponential behavior is the formation of an aggregate species in solution that coexists with the monomer. Further experimental work is underway to more closely examine the nature of the biexponential fluorescence decays. Of the GnOH monodendrons, G2OH has the longest fluorescence lifetime and the highest fluorescence quantum yield. The decrease in the fluorescence lifetimes of G3OH and G4OH correlates with the decrease in their fluorescence quantum yields, suggesting that nonradiative processes begin to compete more effectively with radiative relaxation as the monodendron size increases.

Table 3 shows that the GnPer series exhibits a weak size dependence of the fluorescence lifetime. The shorter fluorescence lifetime shown by the larger generations is likely due to an increased coupling of the perylene trap with the π-electron system of the backbone. This result is in contrast to the fluorescence decays measured for the symmetrical perylene-terminated PA monodendrons, where all generations exhibited nearly the same fluorescence lifetime of about 2.3 ns (in DCM).[2] The all-*meta* branching in the symmetrical monodendrons apparently provides greater isolation of the perylene chromophore from the PA backbone.

Energy Transfer Measurements. The energy transfer quantum efficiency (ϕ_{ET}) of the perylene-terminated monodendrons can be estimated using both steady-state and time-resolved fluorescence measurements.[2,8,9,16] The first method used below relies on a comparison of the absorption spectrum and corresponding fluorescence excitation profile,[8,16,17] which is shown in Figure 11a−d for each member of the GnPer series. The fluorescence excitation profiles were corrected for the lamp spectrum and the instrumental response, and then normalized to best match the absorption spectrum in the perylene region. In each case, the shape and magnitude of the fluorescence excitation profile reasonably approximate the absorption spectrum. The ϕ_{ET} at a specific wavelength is estimated by comparing the intensities of the excitation profile and the absorption spectrum at that wavelength. The ϕ_{ET} over the full absorption spectrum is defined as the ratio of the areas under the fluorescence and absorption profiles. The results for GnPer in DCM are summarized in Table 4. We find that ϕ_{ET}'s typically fall into the 85−95% range at the specific wavelengths shown in Table 4 and the 85−93% range when comparing the areas under the two spectra. These measurements indicate that the energy transfer from the PA antenna to the perylene trap is very efficient over a broad range of absorption wavelengths. The ϕ_{ET}'s determined for the GnPer series are similar to those of the symmetrical compact PA monodendrons. For example, ϕ_{ET} has been estimated to be 91% for monodendron **1**.[2] In contrast, energy transfer quantum yields for the symmetrical extended monodendrons have been estimated to approach unity, $\phi_{ET} \approx$ 98% for **2**.[2] It is possible that steric crowding of the branches in the unsymmetrical monodendrons (due to the *ortho* branching) results in a fraction of the absorbed energy being channeled to other relaxation pathways. It should be emphasized that the

(16) Li, F.; Yang, S. I.; Ciringh, Y.; Seth, J.; Martin, C. H., III; Singh, D. L.; Kim, D.; Birge, R. R.; Bocian, D. F.; Holten, D.; Lindsey, J. S. *J. Am. Chem. Soc.* **1998**, *120*, 10001.
(17) Stryer, L.; Haugland, R. P. *Proc. Natl. Acad. Sci. U.S.A.* **1967**, *58*, 719.

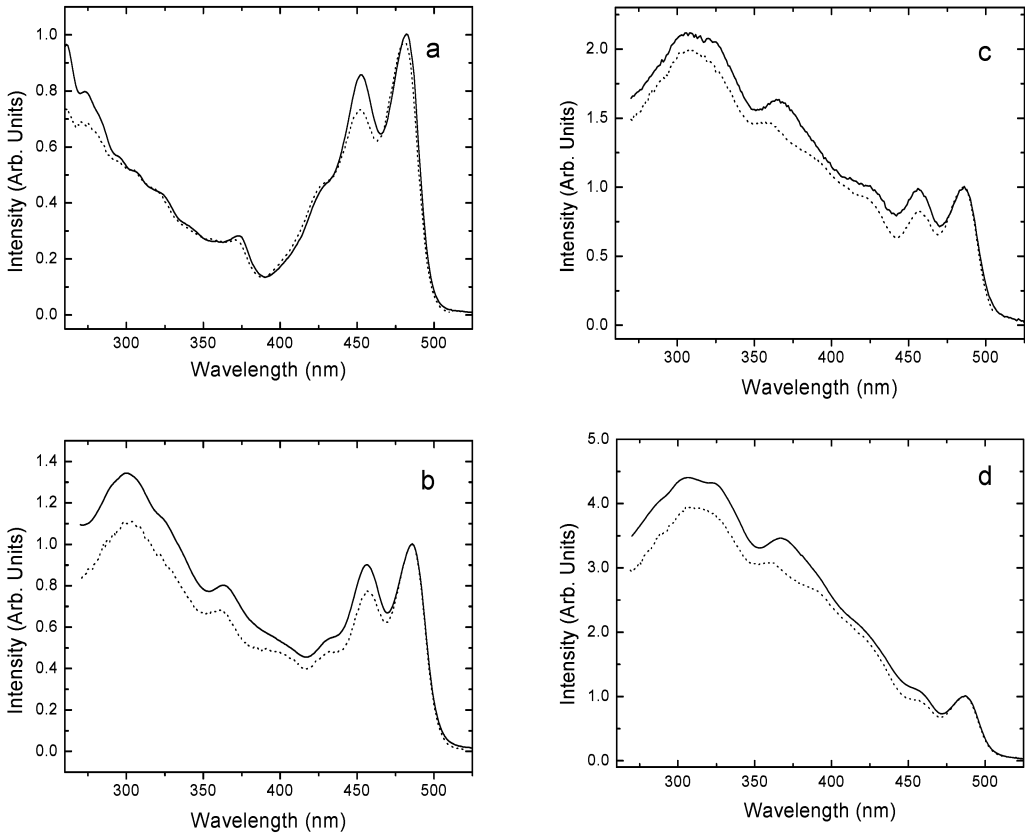

Figure 11. Absorption spectrum (dotted line) and fluorescence excitation profile (solid line) normalized to the absorption spectrum in the perylene region, (a) G1Per, (b) G2Per, (c) G3Per, (d) G4Per. All measurements are in dichloromethane. Each fluorescence excitation profile is measured at an emission wavelength of 530 nm.

Table 4. Energy Transfer Quantum Yields Estimated by Three Methods: (1) Comparing Fluorescence Excitation Profiles with Absorption Spectra, (2) Measurement of Fluorescence Quenching, and (3) Time-Resolved Fluorescence As Described in the Text[a]

		method 1					
compd		*I*(300)/ *I*(max,Per)	*I*(350)/ *I*(max,Per)	*I*(375)/ *I*(max,Per)	ratio of areas	method 2	method 3
	absorption ratio	0.56	0.28	0.28			
G1Per	excitation ratio	0.52	0.27	0.25			
	ϕ_{ET}	0.93	0.96	0.89	0.93	0.99	>0.97
	absorption ratio	1.29	0.77	0.72			
G2Per	excitation ratio	1.10	0.66	0.54			
	ϕ_{ET}	0.85	0.86	0.75	0.85	0.99	>0.97
	absorption ratio	2.07	1.56	1.53			
G3Per	excitation ratio	1.97	1.48	1.33			
	ϕ_{ET}	0.95	0.95	0.87	0.91	0.98	>0.97
	absorption ratio	4.46	3.33	3.25			
G4Per	excitation ratio	3.83	3.06	2.81			
	ϕ_{ET}	0.86	0.92	0.85	0.90	>0.95	>0.97

[a] *I*(max,Per) represents the intensity of the absorption or fluorescence profile at the maximum in the perylene region. All values correspond to the monodendrons dissolved in dichloromethane. Methods 2 and 3 use excitation at 350 nm.

method based on comparing absorption and fluorescence excitation profiles assumes that the fluorescence quantum yield of the perylene trap is independent of the mechanism of excitation, either by direct absorption or by excitation transfer. As pointed out in ref 8, this method also relies on the comparison of data from two different instruments, which can lead to inaccuracies in determining the energy transfer quantum yields especially when they are nearly quantitative.

The second method relies on measuring the fluorescence quantum yield of the donor species in the presence of the perylene trap. This is accomplished by comparing the fluorescence quantum yields of the GnOH samples (which represent the fluorescence quantum efficiency of the donor species) to the fluorescence quantum yields of GnPer in the region where the GnOH compounds emit (the residual fluorescence). On the basis of the measurements shown in Figure 7, and the quantum yields of the donor compounds, the quenching of the emission from the PA backbone region for generations 1−3 was greater than 50-fold, which is consistent with a ϕ_{ET} greater than 98% (for excitation at 350 nm). For G4Per, the quenching is consistent with a ϕ_{ET} greater than 95%.

Previous studies of energy transfer in light-harvesting systems have emphasized that when the energy transfer quantum yields approach unity, time-resolved measurements give more accurate estimates than steady-state measurements.[8,16] If the rise time of the perylene fluorescence can be resolved in the TCSPC measurements, then the following relation can be used to assess the quantum yield:[8]

$$k_{ET} = \frac{1}{\tau_0}\left(\frac{1}{\left(\frac{1}{\phi_{ET}}\right) - 1}\right) \quad (1)$$

where τ_0 is the fluorescence lifetime of the donor compound and the rate of energy transfer, k_{ET}, is associated with the experimentally measured rise time ($1/\tau_{rise}$) of the acceptor (perylene) fluorescence. The instrumental response time of the TCSPC apparatus permits the resolution of roughly 50 ps events. While our instrumental response time was too slow to resolve the fast rise times of the GnPer fluorescence, it can be used to place an upper limit of about 50 ps to the fluorescence rise time. Because the fluorescence lifetimes of the model donor GnOH series were in the 1.7−2.0 ns range, it follows that a lower limit for the ϕ_{ET} is nearly 97% using this method (for excitation at 350 nm). Clearly, it would be desirable to have ultrafast measurements of the fluorescence rise time to obtain a more accurate number for ϕ_{ET}.

The three methods described above are in fair agreement. The method based on comparing the excitation and absorption spectra gives somewhat lower estimates for the energy transfer quantum yield. Taken together, the three methods show that the energy transfer quantum yields are very high for GnPer (at least up to the fourth generation in size). Furthermore, they compare favorably to the energy transfer quantum yields exhibited by other light-harvesting dendritic and nondendritic systems.[2−4,8,9,16]

Ultrafast Dynamics. An initial measure of the excited-state dynamics of the G3 monodendrons in DCM was obtained using the technique of ultrafast pump−probe spectroscopy. In this technique, a pump pulse transfers a portion of the ground-state population onto the excited-state surfaces, and the probe pulse measures the recovery of the ground state and, possibly, the dynamics of any excited-state transitions that overlap the probe bandwidth. Figure 12a,b shows representative pump−probe transients for G3OH and G3Per, respectively. At 310 nm, the pump pulse (175 fs) excites a superposition of states within the dendritic backbone. In each case, the signal at $t > 0$ is a transient bleach; that is, the transmission of the probe pulse is higher due to the excitation produced by the pump. The abscissa represents the normalized change in sample transmission, $\Delta T/T$, or $(T_f - T_i)/T_i$, where T_f represents the probe fluence transmitted through the sample, and T_i represents the incident probe fluence.

Figure 12a shows that ultrashort pulsed excitation of G3OH results in a bleach signal that reveals at least two decay components within the experimental time window. The solid line in Figure 12a is a fit based on the sum of two exponential decay functions. The fast component relaxes with a time constant of 6.0 ± 1.0 ps, while the slow component has a time constant greater than 100 ps. If a superposition of states associated with different PA structures is initially excited by the pump, it is expected that the electronic excitations will funnel to the PA main branch, which forms the lowest energy state. In this picture, the faster component is suggested to indicate the recovery time of the ground electronic states associated with the initially pumped PA structures. The origin of the longer component is not yet clear and must be characterized using a longer experimental time window.

Figure 12b shows that the attachment of the perylene trap to the G3 monodendron dramatically shortens the characteristic decay times of the bleach signal. In the time window examined, the transient bleach signal also reveals two relaxation components. A fit to the sum of exponential decay functions yields a time constant of 400 ± 50 fs for the fast component, and 18 ± 4.0 ps for the slower component. Clearly, the addition of the perylene trap acts as a strong driving force to funnel energy from the PA backbone, which leads to a shortening of the relaxation dynamics by at least 1 order of magnitude. Given that the energy transfer quantum yield is quite high (≳90%) for G3Per in DCM, we suggest that the shortening of its transient bleach signal relative to G3OH is primarily due to an energy transfer mechanism that occurs on an ultrashort time scale. It is important to emphasize, however, that our evidence is only suggestive, because the measurement of a ground state recovery does not directly measure the induction of population into the perylene trap. A direct measure of the energy trapping time may be obtained through multicolor pump−probe experiments, or by measuring the rise time of the perylene fluorescence using femtosecond fluorescence gating techniques.[18]

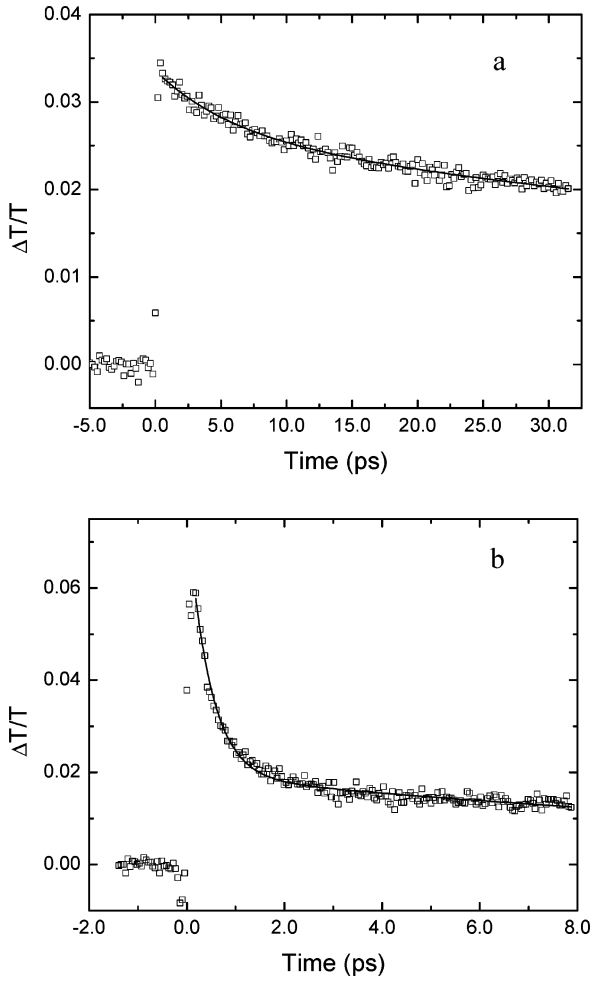

Figure 12. Transient bleach signals for 175 fs pulsed excitation at 310 nm. The signal is plotted as the normalized change in transmission, $\Delta T/T$. (a) G3OH in dichloromethane and (b) G3Per in dichloromethane. The solid line is a fit to the data based on a sum of two exponentials. The decay time of the fast component is 6.0 ± 1.0 ps for case a, and 400 ± 50 fs for case b.

Energy Transfer Mechanisms. On the basis of the results shown above, the energy transfer from the PA backbone to the perylene trap occurs rapidly and is completed in a time frame of less than about 100 ps. The ultrafast pump−probe results

(18) Kinoshita, S.; Ozawa, H.; Kanematsu, Y.; Tanaka, I.; Sugimoto, N.; Fujiwara, S. *Rev. Sci. Instrum.* **2000**, *71*, 3317.

suggest that (for G3Per) there is a component of the energy transfer that occurs on a subpicosecond time scale. In principle, singlet−singlet energy transfer can proceed by a through-space Coulombic mechanism (Förster energy transfer),[19] as well as a through-bond mechanism that depends on short-range orbital interactions.[20,21] The coupling of the perylene trap to the PA backbone through an ethynyl linkage suggests that a through-bond mechanism may make a dominant contribution to the energy transfer rate. However, the large molar absorptivity, the high fluorescence quantum yields of the monodendron donor compounds, and the good spectral overlap of the GnOH fluorescence with the perylene absorption suggest that a Coulomb-based mechanism may also contribute substantially to the energy transfer rate. The total electronic coupling between the donor and acceptor can be written as the sum of through-space (Coulomb) and through-bond interactions[22]

$$V = V_{\mathrm{Coul}} + V_{\mathrm{TB}} \tag{2}$$

and the rate of energy transfer given by[22]

$$k_{\mathrm{ET}} = \frac{2\pi}{\hbar}|V|^2\rho_{\mathrm{E}} \tag{3}$$

where ρ_{E} is the density of states appropriate to the electronic energy transfer. Previous studies have determined the relative contributions of the two mechanisms by calculating the energy transfer rate constant due to the through-space mechanism in the point dipole approximation and by comparing the calculated rate to the experimentally measured energy transfer rate constant.[16,22] Before such an approach can be applied in a meaningful way to the results of this work, some additional experimental work and theoretical modeling are necessary. First, an accurate measurement of the time scale of the energy transfer to the perylene trap must be made using ultrafast spectroscopy, as described above. Experimental work is in progress in our laboratory to measure the energy trapping times for the GnPer series. Second, to estimate the through-space contribution to the energy transfer rate constant, the donor−acceptor separation distance must be determined.

Conclusions

In this paper, we have described the optical and photophysical properties of a new class of phenylacetylene monodendrons characterized by unsymmetrical branching. Monodendrons through the fourth generation are studied both with and without a fluorescent perylene trap covalently attached at the core. It is found that the unsymmetrical branching leads to optical and photophysical properties that are substantially different than those of phenylacetylene monodendrons based on symmetrical branching. Most notably, the unsymmetrical branching gives rise to very broad absorption spectra for the higher generation monodendrons. For example, the G4OH dendrimer has an absorption cross section that covers a range greater than 200 nm (~18 000 cm^{-1}) and is significantly broader than either the fourth generation symmetrical compact or the extended PA monodendrons. Furthermore, as the generation number increases for the unsymmetrical monodendrons, it is found that the amount of light absorbed approximately doubles for each generation. The peak molar absorptivity for G4OH exceeds 3×10^5 M^{-1} cm^{-1} (at 305 nm), and significant light absorption is maintained to about 450 nm, which confirms that it is an efficient light-absorbing antenna in the near UV and blue parts of the spectrum. We anticipate that larger generations will exhibit even larger molar absorptivities and thus act as even more efficient antennae, although the red shift in the absorption is expected to saturate in the vicinity of 500 nm (on the basis of the absorption edges typically shown by rigid-rod phenylene ethynylene polymers).[23]

The fluorescence quantum yields for both the GnOH and the GnPer series varied from 65 to 81%, which compare favorably to other light-harvesting systems.[2,8,9,16] The GnOH series showed only a minor shortening of the fluorescence lifetime with monodendron size as the generation number is increased from 2 to 4, which suggests that higher generations may also have substantial fluorescence quantum yields. The energy transfer quantum yields were estimated using both steady-state and time-dependent spectroscopy. Notably, Figure 7 shows that when the excitation wavelength is tuned to excite predominantly the phenylacetylene backbone, the fluorescence emission comes almost entirely from the perylene trap, with little residual emission from the backbone states. If the results of the steady-state and time-dependent measurement techniques are averaged, it is found that for all of the generations the energy transfer quantum yields exceed 93%. It will be interesting to see if larger perylene-terminated generations ($n > 4$) maintain high energy transfer quantum efficiency.

Questions remain regarding the nature of the electronic excitations within the phenylacetylene backbone and the mechanism by which electronic energy is directed to the perylene trap. While there is some spectroscopic evidence for localized electronic excitations, additional experimental work, as well as theoretical calculations, will be needed to clarify this issue. A better understanding of the electronic structure will also help in understanding the nature of the energy funneling process within the dendritic backbone and the mechanism of energy transport to the core.

Finally, we mention that the properties of spectrally broad absorption cross sections, large molar absorptivities, high fluorescence quantum yields, and high energy transfer quantum yields exhibited by the unsymmetrical phenylacetylene monodendrons make them potentially attractive candidates as materials for a variety of molecular-based photonics devices.

Acknowledgment. The authors thank the Office of Naval Research for support of this research.

JA020380J

(19) Förster, T. *Ann. Phys.* **1948**, *2*, 5.
(20) Dexter, D. L. *J. Chem. Phys.* **1953**, *21*, 836.
(21) Ghiggino, K. P.; Yeow, E. K. L.; Haines, D. J.; Scholes, G. D.; Smith, T. *J. Photochem. Photobiol., A* **1996**, *102*, 81.
(22) Scholes, G. D.; Ghiggino, K. P.; Oliver, A. M.; Padden-Row, M. N. *J. Phys. Chem.* **1993**, *97*, 11871.
(23) Moroni, M.; LeMoigne, J.; Pham, T. A.; Bigot, J. Y. *Macromolecules* **1997**, *30*, 1964.